Chen-Hu, K., Liu, Y. & Armada, A. G. (2020). Non-Coherent Massive MIMO-OFDM Down-Link Based on Differential Modulation. *IEEE Transactions on Vehicular Technology*, 69(10), pp. 11281–11294.

DOI: 10.1109/tvt.2020.3008913

Non-Coherent Massive MIMO-OFDM Down-Link based on Differential Modulation

Kun Chen-Hu, *Student Member, IEEE,* Yong Liu, and Ana García Armada, *Senior Member, IEEE*

***Abstract*—Orthogonal frequency division multiplexing (OFDM) and multiple-input multiple-output (MIMO) are wireless radio technologies adopted by the new Fifth Generation (5G) of mobile communications. A very large number of antennas (massive MIMO) is used to perform the beam-forming of the transmitted signal, either to reduce the multi-user interference (MUI), when spatially multiplexing several users, or to compensate the path-loss when higher frequencies than microwave are used, such as the millimeter-waves (mm-Waves). Usually, a coherent demodulation scheme (CDS) is used in order to exploit MIMO-OFDM, where the channel estimation and the pre/post-equalization processes are complex and time consuming operations, which require a considerable pilot overhead and also increase the latency of the system. As an alternative, non-coherent techniques based on a differential modulation scheme have been proposed for the up-link (UL). However, it is not straightforward to extend these proposals to the down-link (DL) due to the (usually) reduced number of antennas at the receiver side. In this paper we overcome this problem, and assuming that each user equipment (UE) is only equipped with one single antenna, we propose the combination of beam-forming with a differential modulation scheme for the DL, enhanced by the frequency diversity. The new transmission and reception schemes are described, and the signal-to-interference-plus-noise ratio (SINR) and the complexity are analysed. The numerical results verify the accuracy of the analysis and show that our proposal outperforms the existing CDS with a significant lower complexity.**

I. Introduction

The Fifth Generation (5G) of mobile communication systems [1] is one of the most ambitious projects developed by industry and academia in several decades. The 5G (and beyond) will have to cope with a great variety of heterogeneous communications services in many completely different scenarios [2]. The main use cases can be summarized as enhanced mobile broadband (eMBB), massive machine type communications (mMTC) and ultra reliable low-latency communications (URLLC). Unlike the previous generations, the future ones not only need to provide a high data rate/throughput, but other requirements must also be fulfilled such as improved coverage, lower latency, high mobility, high reliability and lower infrastructure costs [3].

Kun Chen-Hu and Ana García Armada are with Deparment of Signal Theory and Communications of Universidad Carlos III of Madrid (Spain). E-mails: {kchen, agarcia}@tsc.uc3m.es.

Yong Liu is with Shanghai Research Center, Huawei Technologies (China). E-mail: liu.liuyong@huawei.com.

This work has been funded by project TERESA-ADA (TEC2017-90093-C3-2-R) (MINECO/AEI/FEDER, UE).

Recently, the Third Generation Partnership Project (3GPP) has published the first versions of the standard for the 5G new radio (NR) [1], where multiple-input multiple-output (MIMO) systems [4] with orthogonal frequency division multiplexing (OFDM) [5] are set as the radio techniques for the physical layer. In order to increase the data rate and implement several new services, higher frequency bands than in previous generations are proposed to be exploited to obtain more available bandwidth, such as 3.5 GHz and millimeter-waves (mm-Waves) [6]. Due to the higher path-loss of these bands, they have not been massively exploited for mobile communications in the past. Nevertheless, satellite communications, wireless back-haul and radar applications are some examples of previous use of mm-Waves. Additionally, the complexity of the signal processing techniques needs to be bounded due to the fact that it will reduce the cost of the devices and the delay of the required operations, fulfilling some of the requirements of mMTC and URLLC.

The use of beam-forming, creating a steerable radiation pattern, is not only required to overcome the increased path-loss at higher frequency bands, but also to spatially multiplex multiple users [7]. Fully digital beam-forming architectures [8] are able to provide a good flexibility and a high performance. However, when the number of antennas is very large, the high number of required radio-frequency chains with their analog to digital or digital to analog converters will increase the cost and the power consumption of the system. Therefore, hybrid analog-digital beam-forming [9] is an elegant solution capable of reducing the hardware elements, where a digital processing unit is in charge of the digital beam-forming and the analog beam-forming is usually implemented with a phased-array. Moreover, in order to improve the performance of the beam-forming, different techniques are proposed, such as optimization of the beam-pattern [10], joint bit allocation and beam-forming optimization [11], dynamic radio-frequency chain selection [12] and antenna selection [13].

Traditionally, a coherent demodulation scheme (CDS) is used in order to fully exploit the benefits of MIMO-OFDM, where the channel state information (CSI) is obtained from reference signals at the cost of some overhead [14]–[16]. The channel estimation procedure in MIMO systems for the computation of the pre/post-coding matrices depends on the duplexing mode [17], namely frequency division duplexing (FDD) or time division duplexing (TDD). In the case of TDD, each user equipment (UE) in a cell transmits its allocated orthogonal sequence to the base station (BS) (if sequences are not orthogonal, pilot contamination will arise), and the latter is in charge of obtaining the channel estimation and computing

the pre/post-coding matrices. Then, channel reciprocity is assumed, where the response of the channel is the same for both up-link (UL) and down-link (DL), and therefore, the computed pre/post-coding matrices are valid for both links. However, the different radio-frequency chains connected to the UL and DL have their own responses, and a calibration process is required [18] in order to estimate and compensate this additional effect. In the case of FDD, the channel estimation for the UL is similar to TDD. However, the channel response for the DL cannot be inferred from the UL, and it must be also estimated. The BS transmits orthogonal sequences to all UEs of the cell, and these UEs estimate their corresponding channel response and feed them back to the BS in order to compute the pre-coding matrices, or alternatively feed back some indication of a selected precoder from a reduced set. The overhead in the UL training is related to the number of UEs, while it is proportional to the number of BS antennas in the DL training, which is usually higher. Then, TDD is preferable due to the fact that it requires a lower overhead for the channel estimation of both links. Nevertheless, the large majority of cellular networks deployed today make use of FDD, where new techniques are required to improve its performance. And even in the case of TDD, the overhead produced by the reference signals may be significant due to the fact that an accurate-enough channel estimation is required in the whole time-frequency resource grid, especially for fast-varying and/or very frequency-selective channels, where the CSI must be frequently updated in the time and frequency dimensions. Besides CSI estimation, the channel equalization process may become more complex when a massive number of antennas is considered. For example, the channel inversion of large dimension matrices is prohibitive when a zero-forcing (ZF) criterion is chosen. Although, there are different numerical approximations [19] to alleviate the complexity of the matrix inversion, the computation of the equalizers still must be performed for each resource block of the grid. On the other hand, the quality of the equalizers can be easily degraded by some undesirable effects such as out of cell multi-user interference (MUI), noise or correlation among antennas. Lastly, independently of whether precoding is used, CDS requires channel estimation at the receiver, be it the BS or the UE, with the adequate training overhead.

Hence, in order to implement MIMO-OFDM with a large number of antennas, especially in FDD, 5G NR proposes an alternative way consisting of two steps. Firstly, the beam-management procedure [20] is responsible of accurately determining the angle of the spatial clusters of the propagation channel contributing to the signal of each UE. Then, in the DL, the BS transmits one or several data streams with the corresponding reference signals to each UE by using beam-forming [7], focusing the energy in the determined specific directions in order to compensate, as far as possible, the path-loss and avoid the MUI by spatially multiplexing the UEs in different beams. Similarly, beam-forming is used in the UL for the BS to receive the signal coming from the determined spatial directions.

A. Literature review

Alternatively, non-coherent detection schemes (NCDS) have been proposed in order to avoid the channel estimation and equalization processes for massive MIMO systems. In the context of UL, [21]–[27] propose to transmit with the single antenna of each UE and exploit the spatial diversity at the BS provided by its large number of antennas in order to improve the performance. Reference [21] proposed a NCDS based on amplitude shift keying (ASK), which is able to asymptotically achieve the same performance as an equivalent CDS. However, it requires a very large number of antennas to get an acceptable performance. Reference [22] combines the energy detection with deep neural networks. Then, [23]–[26] proposed the use of differential phase shift keying (DPSK), where the BS non-coherently combines two contiguously transmitted symbols for each antenna, and performs an averaging process over the spatial domain in order to mitigate the effects of the channel. Moreover, they proposed the idea of multiplexing different UEs in the constellation domain based on a joint-symbol, which is a superposition of the symbols of several UEs. Reference [28] proposed some constellations that enable multiplexing different UEs, however, only two UEs are supported. Later, the combination of [23] with OFDM is studied in [27] assuming a doubly dispersive channel model. With the inclusion of OFDM, two contiguous differential symbols can be placed either in time or frequency domain. It was shown that although the time domain scheme has a straightforward implementation, the latency is increased due to the need to wait at least for one complete OFDM symbol in order to perform the differential demodulation at the receiver. In the frequency domain scheme, the latency is negligible while an additional common phase error must be estimated and corrected.

In the context of DL, the combination of NCDS with MIMO has been until now based on coding, with schemes such as differential unitary space-time modulation (DUSTM) [29], differential space-time block codes (DSTBC) [30] and Grassmannian codes (GC) [31], [32]. All the mentioned techniques transmit the designed constellations and code blocks using different antennas at the BS and several channel uses (time instants), where the number of channel uses must be, at least, equal to the number of antennas at the transmitter. However, they require that the channel response not only remains quasi-static during the transmission of a code block, but also it must be spatially uncorrelated. DUSTM and DSTBC are an extension of the DPSK to several antennas at the transmitter and the well-known STBC [33], respectively. GC is the best of them in terms of achievable rate, due to the fact that it assumes that the space spanned by the transmitted matrices is invariant to the channel matrix. However, it requires that the signal-to-noise ratio (SNR) is very high. In any case, when the number of antennas at the BS is very large, the design of constellation and/or code blocks for all these techniques becomes unaffordable. In [34], a comparison of different schemes is provided, where only two and four transmit antennas are taken into account. For this setting, the results show that GC slightly outperforms the other schemes in low-Doppler shift scenarios.

In summary, the techniques provided in the literature, either

for UL or DL, can not be straightforwardly extended to the scenario of massive MIMO in the DL. The lack of channel estimation in [23]–[27] requires multiple antennas at the receiver to obtain a SNR gain, which may not be placed generally in the UE. Furthermore, [29]–[32] not only cannot make use of the availability of a large number of antennas at the BS, but also do not perform well in fast-varying and/or frequency-selective channels, which are of interest in the context of 5G.

B. Contributions

In this paper, we propose the combination of the NCDS with beam-forming for the DL, where a certain channel knowledge is needed to point the beam towards the UE through the beam-management procedure, and the signal is processed non-coherently in each beam afterwards. Hence, the large number of antennas at the BS is used for compensating the path-loss and enhancing the quality of the link. A beam-management procedure similar to the 5G NR procedure [20] is assumed to be performed prior to the transmission. Additionally, inspired by [23], we also propose to average in another dimension rather than the spatial, namely the frequency domain, for those services which are critical in terms of performance. This averaging process is suitable for a performance versus rate trade-off, and can be easily configured according to the requirements of the higher layers. For this combination of beam-forming and NCDS, we provide some analytical expressions of the signal-to-interference-plus-noise ratio (SINR), a study of the complexity and some numerical results to show the benefits of our proposal as compared as the traditional CDS.

The main contributions of this paper are as follows:

- We propose a feasible way of performing NCDS in the DL making use of the large number of antennas at the BS. None of the existing schemes in the literature can exploit this property due to the fact that coding-based techniques have a prohibitive complexity, even for a moderate number of antennas. Our proposal is based on the differential modulation scheme in combination with the beam-management procedure of 5G, which is capable of mitigating the effects of path-loss and improving the interference reduction when the number of antennas is large enough. Moreover, the performance of our proposal is better than the use of the traditional CDS in most of the analyzed cases, for both sub-6 GHz and mm-Waves bands. The proposed NCDS does not require any CSI at either transmitter or receiver additional to the standard beam-management procedure. Only in the case of combining it with OFDM for very frequency-selective channels, just two pilots are needed for the phase correction of many consecutive OFDM symbols, which is a negligible overhead.
- We provide an analytical expression of the SINR for the particular case of DL, assuming a geometric wideband channel model [35]–[37] and multi-user (MU) scenario, where each UE is exploiting the frequency diversity at the receiver, since the antenna diversity is limited due to its single-antenna reception. Note that [23] and [27] provide the SINR expression assuming a spatially uncorrelated flat-fading and frequency-selective channel, respectively, for the particular case of UL where the spatial diversity is exploited at the BS receiver, which is not possible in the single-antenna receivers of the DL. Our analytical derivations are shown to match well with the simulation results, and can be used for the system design and to develop scheduling algorithms [38].
- A complexity analysis comparison among our proposed technique and the traditional CDS based on ZF and maximum ratio transmission (MRT) is provided, showing that our proposal is less complex than CDS for different 5G scenarios.

The remainder of the paper is organized as follows. Section II provides the system model of multi-user (MU) MIMO-OFDM for the DL scenario and the differential modulation scheme. Section III describes our proposed NCDS based on frequency diversity combined with beam-forming for the MU case. Section IV provides the analytical expression of the SINR. Section V describes the analysis of the complexity. Section VI presents some numerical results to verify our theoretical analysis and provides a better understanding of the system performance as compared to the traditional CDS. Finally, in section VII, some conclusions are pointed out.

Notation: matrices, vectors and scalar quantities are denoted by boldface uppercase, boldface lowercase, and normal letters, respectively. $[\mathbf{A}]_{m,n}$ denotes the element in the m-th row and n-th column of $\mathbf{A}$. $[\mathbf{a}]_n$ represents the n-th element of vector $\mathbf{a}$. $\mathbf{I}_M$ is the identity matrix of size $M \times M$. $\mathbf{0}_{M,N}$ is the zero matrix of size $M \times N$. $\mathbf{1}_{M,N}$ denotes a matrix of ones of size $M \times N$. The superscripts $(\cdot)^T$,$(\cdot)^H$ and $(\cdot)^*$ denote transpose, hermitian and complex conjugate operations, respectively. $\mathbb{E}\{\cdot\}$ represents the expected value. $\mathcal{CN}(0,\sigma^2)$ represents the circularly-symmetric and zero-mean complex normal distribution with variance σ^2. $||\cdot||_F^2$ denotes the squared Frobenius norm.

II. System Model

For the sake of conciseness and ease of understanding, in Table I, we provide the summary of the most frequently used acronyms in the paper.

We consider one BS equipped with an array of V transmit antennas and U UEs with one single receive antenna each. The angular position of the UEs is determined by its azimuth angle, which is denoted as $\theta^u_{\text{UE}} \in [-\pi/2, \pi/2)$ and we assume that it is unknown to the BS. For simplicity, we assume that the elevation angles of all UEs are the same, and hence, this parameter is not taken into account in the system model. We focus on the DL, where the BS transmits M consecutive OFDM symbols to each UE. The OFDM signal has K subcarriers and the length of the cyclic prefix (L_{CP}) is long enough to absorb the effects of the multi-path channel. At the UE, after removing the cyclic prefix and performing a fast-Fourier transform (FFT), we can process each subcarrier as one of a set of K independent sub-channels.

A. Transmitter

At the transmitter, the beam-formed data for the k-th subcarrier and m-th OFDM symbol $\mathbf{x}^m_k$ of size $(V \times 1)$ is given

TABLE I
ACRONYMS

Acronym	Description
AS	Angular spread
BLER	Block error rate
BS	Base station
CDS	Coherent demodulation scheme
DL	Down-link
DS	Delay spread
EE	Energy efficiency
MIMO	Multiple-input multiple-output
MRT	Maximum ratio transmission
MU	Multi-user
MUI	Multi-user interference
NE	Non-estimation
NCDS	Non-coherent demodulation scheme
NRM	Number of real multiplication
OFDM	Orthogonal frequency division multiplexing
PE	Perfect estimation
PMI	Precoding matrix indicator
PSK	Phase shift keying
RE	Realistic estimation
SER	Symbol error rate
SINR	Signal to interference plus noise ratio
SNR	Signal to noise ratio
SU	Single user
UE	User equipment
UL	Up-link
ZF	Zero-forcing

as

$$\mathbf{x}_k^m = \mathbf{B}\check{\mathbf{s}}_k^m, \tag{1}$$

$$\mathbf{B} = \begin{bmatrix} \mathbf{b}_1 & \cdots & \mathbf{b}_U \end{bmatrix}, \tag{2}$$

$$\check{\mathbf{s}}_k^m = \begin{bmatrix} \left[\mathbf{s}_1^m\right]_k & \cdots & \left[\mathbf{s}_U^m\right]_k \end{bmatrix}^T, \tag{3}$$

where $\mathbf{B}$ denotes the $(V \times U)$ beam-forming matrix and $\mathbf{s}_u^m$ represents the differential data stream $(K \times 1)$ vector transmitted to the u-th UE. Note that they must satisfy the power constrains given by

$$||\mathbf{b}_u||_F^2 = 1, \quad \left\|\mathbf{s}_u^m\right\|_F^2 = \sqrt{p_u}, \quad \sum_{u=1}^{U} p_u \leq 1. \tag{4}$$

Then, each OFDM symbol to be transmitted in the time domain $\tilde{\mathbf{x}}_v^m$ of size $((K + L_{CP}) \times 1)$ per antenna $(v = 1, \cdots, V)$ can be built as

$$\tilde{\mathbf{x}}_v^m = \mathbf{E}\mathbf{F}_K^H \check{\mathbf{x}}_v^m, \tag{5}$$

$$\check{\mathbf{x}}_v^m = \begin{bmatrix} \left[\mathbf{x}_1^m\right]_v & \cdots & \left[\mathbf{x}_K^m\right]_v \end{bmatrix}^T, \tag{6}$$

where $\mathbf{F}_K$ and $\mathbf{E}$ are the FFT and cyclic prefix matrices, respectively, defined as

$$[\mathbf{F}_K]_{k_1,k_2} = \frac{1}{\sqrt{K}} \exp\left(-j\frac{2\pi}{K}(k_1 - 1)(k_2 - 1)\right), \tag{7}$$

$$\mathbf{E} = \begin{bmatrix} \mathbf{E}_{CP} & \mathbf{I}_K \end{bmatrix}^T, \quad \mathbf{E}_{CP} = \begin{bmatrix} \mathbf{0}_{L_{CP} \times (K - L_{CP})} & \mathbf{I}_{L_{CP}} \end{bmatrix}^T. \tag{8}$$

Note that $\mathbf{B}$ remains invariant for M consecutive OFDM symbols and all subcarriers due to the fact that the instantaneous channel response is unknown. Hence, $\mathbf{B}$ only points the energy to the angular position of different UEs, and these angles are quasi-static parameters that are found through the beam-management procedure.

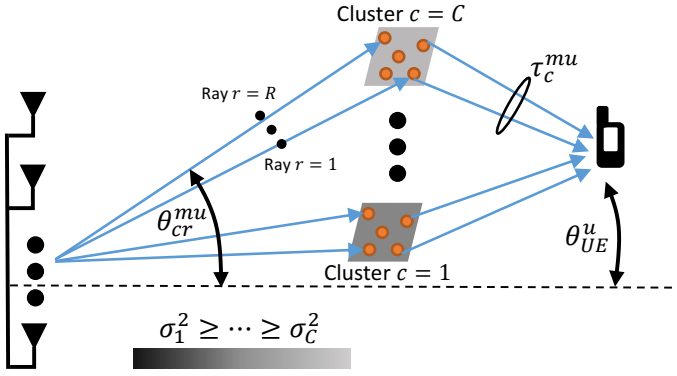

Fig. 1. Channel model.

B. Channel model

The use of higher frequencies can leverage the large bandwidths available at 3.5 GHz band and mm-Waves spectrum between [30 – 300] GHz to provide high data rates. Channel measurements have confirmed the feasibility of these bands for the deployment of mobile communication systems [35]–[37]. Measurements did not only show that the path-loss is higher, but also the energy arrives in clusters from multiple distinct angular directions, presumably through different scattering or reflection paths. To incorporate the wideband and limited scattering characteristics of channels at higher frequencies, we adopt a geometric wideband channel model which enables the characterization of the effects of the propagation channel and the antenna arrays [35]–[37]. It is characterized by the geometric superposition of several separate clusters, where each of them has a different value of delay and gain. Moreover, each cluster is made of a certain number of rays with different angle of arrival and departure. Then, in order to obtain the instantaneous channel coefficients, the array steering vectors of both transmitter and receiver are taken into account, where the typical array configurations are linear, rectangular or circular.

The channel model adopted in this work is illustrated in Fig. 1, [39], [40]. Let $\mathbf{H}_k^m$ represent the $(U \times V)$ MIMO channel matrix in the frequency domain, for the k-th subcarrier and m-th OFDM symbol. It can be defined as

$$\mathbf{H}_k^m = \begin{bmatrix} \mathbf{h}_k^{m1} & \cdots & \mathbf{h}_k^{mU} \end{bmatrix}^T, \tag{9}$$

where

$$\left[\mathbf{h}_k^{mu}\right]_v = \sum_{c=1}^{C}\sum_{r=1}^{R} \alpha_{cr}^{mu} \left[\mathbf{a}\left(\theta_{cr}^{mu}\right)\right]_v \exp\left(-j\frac{2\pi}{K}(k-1)\tau_c^{mu}\right), \tag{10}$$

where we assume that there are C clusters for each UE and for each cluster there are R rays. Focusing in a particular UE, all rays of the same cluster have the same time delay τ_c^{mu} expressed in samples. The parameters α_{cr}^{mu} and θ_{cr}^{mu} are the channel complex gain and azimuth angle of departure for the r-th ray in the c-th cluster, respectively; and $\mathbf{a}(\theta)$ denotes the array steering vector of size $(V \times 1)$. In order to provide a better understanding of our proposal, we exemplify our array

configuration as a uniform linear array (ULA). Hence, the expression of $\mathbf{a}(\theta)$ is given by

$$\mathbf{a}(\theta) = \frac{1}{\sqrt{V}} \begin{bmatrix} 1 & e^{j\frac{2\pi d}{\lambda}\cos(\theta)} & \cdots & e^{j\frac{2\pi d}{\lambda}(V-1)\cos(\theta)} \end{bmatrix}^T, \tag{11}$$

where λ is the wavelength and d corresponds to the distance between two contiguous antennas. Additionally, we assume that all UEs have the same power delay profile for the easiness of notation, and that

$$\alpha_{cr}^{mu} \sim \mathcal{CN}\left(0, \sigma_c^2/R\right), \quad \sum_{c=1}^{C} \sigma_c^2 = 1, \quad \sigma_1^2 \geq \cdots \geq \sigma_C^2. \tag{12}$$

Regarding the channel response, we assume that the angles and delays introduced by the clusters are slowly-varying components (θ_{cr}^u and τ_c^u), and they remain constant for the M consecutive OFDM symbols. On the other hand, the fading coefficients (α_{cr}^{mu}) may be fast-varying. [1]

C. Receiver

At the receiver, after removing the cyclic prefix and performing the FFT, the received signal at the k-th subcarrier and m-th OFDM symbol is given by

$$\mathbf{y}_k^m = \mathbf{H}_k^m \mathbf{x}_k^m + \mathbf{w}_k^m = \mathbf{H}_k^m \mathbf{B} \check{\mathbf{s}}_k^m + \mathbf{w}_k^m, \tag{13}$$

where $\mathbf{w}_k^m$ $(U \times 1)$ denotes the additive white Gaussian noise (AWGN) distributed according to $\left[\mathbf{w}_k^m\right]_u \sim \mathcal{CN}(0, \sigma_{w^u}^2)$. Given (13), we focus on the signal of the u-th UE whose expression is

$$\begin{aligned} \left[\mathbf{y}_k^m\right]_u = & \underbrace{\left(\mathbf{h}_k^{mu}\right)^T \mathbf{b}_u \left[\mathbf{s}_u^m\right]_k}_{\text{desired signal}} + \underbrace{\left[\mathbf{w}_k^m\right]_u}_{\text{noise}} + \\ & \underbrace{+ \left(\mathbf{h}_k^{mu}\right)^T \sum_{\substack{u'=1 \\ u' \neq u}}^{U} \mathbf{b}_{u'} \left[\mathbf{s}_{u'}^m\right]_k}_{\text{MUI}}. \end{aligned} \tag{14}$$

Due to the fact that the transmitted streams to the different UEs are uncorrelated to each other and using the central limit theorem (CLT) [41], (14) can be rewritten as

$$\left[\mathbf{y}_k^m\right]_u = \check{h}_k^{mu} \left[\mathbf{s}_u^m\right]_k + \left[\check{\mathbf{w}}_k^m\right]_u, \quad \check{h}_k^{mu} = \left(\mathbf{h}_k^{mu}\right)^T \mathbf{b}_u, \tag{15}$$

where $\check{h}_k^{mu}$ is the equivalent channel response including the effect of the beam-forming, and $\check{\mathbf{w}}_k^m$ $(U \times 1)$ accounts for the joint MUI and noise vector, where each element is distributed according to $\left[\check{\mathbf{w}}_k^m\right]_u \sim \mathcal{CN}(0, \sigma_{\check{w}^u}^2 = \sigma_{i^u}^2 + \sigma_{w^u}^2)$ and

$$\sigma_{i^u}^2 = \sum_{\substack{u'=1 \\ u' \neq u}}^{U} p_{u'} \sum_{c=1}^{C} \frac{\sigma_c^2}{R} \sum_{r=1}^{R} \left(\mathbf{a}^T\left(\theta_{cr}^u\right) \mathbf{b}_{u'}\right)^2. \tag{16}$$

We can see that the power of the MUI is scaled by the allocated power ($p_{u'}$) of other UEs and the correlation among the array steering vector of each cluster of the UE of interest ($\mathbf{a}\left(\theta_{cr}^u\right)$) and the beam-forming vector of other UEs ($\mathbf{b}_{u'}$). Hence, power allocation and UE selection algorithms are needed in order to keep (16) as low as possible [38].

[1] Even though in this paper we do not show the performance in time-varying channels, it has been shown in [24] that the non-coherent DPSK-based massive MIMO is very robust to the time variability of the channel.

D. Differential modulation scheme based on a frequency domain scheme

Similarly to [23]–[27], we also propose the DMS for the implementation of a NC system, now in the DL scenario. Given a vector of complex symbols $\mathbf{r}^{mu}$ to be transmitted to the u-th UE in the m-th OFDM symbol of size $((A-1)\times 1)$, where each element belongs to a PSK constellation of any order, the DPSK symbols $\mathbf{r}_d^{mu}$ of size $((A \times 1))$ in order to be transmitted can be obtained as

$$\left[\mathbf{r}_d^{mu}\right]_{a+1} = \left[\mathbf{r}_d^{mu}\right]_a \left[\mathbf{r}^{mu}\right]_{a+1}, \quad 1 \leq a \leq A-1, \tag{17}$$

where $\left[\mathbf{r}_d^{mu}\right]_1$ is a known reference symbol. In the following section, we will provide the details of how to map the differential symbols $\mathbf{r}_d^{mu}$ into the OFDM resource grid $\mathbf{s}_u^m$, and the relation between parameters K and A.

III. Proposed MU Scheme for the DL

According to [23]–[27], the differential modulation scheme requires some diversity at the receiver side, where the interference and noise terms can be effectively averaged out. In UL, this diversity is exploited in the spatial dimension at the BS, where the uncorrelated received signals of all antennas are non-coherently combined to produce a good estimation of the transmitted complex symbols. Moreover, in order to support a MU scenario, the data of several UEs are multiplexed in the constellation domain, where the BS receives a joint-symbol which is a superposition of the transmitted symbol of each UE.

However, for the particular case of DL, the required averaging process for the differential modulation scheme can not be performed over the spatial domain, due to the fact that the UEs usually have a reduced number of antennas and are, in particular, constrained to be equipped with a single antenna in this work. Additionally, regarding the MU scenario, the proposed constellation multiplexing technique is limited, due to the fact that it only supports up to two UEs for reasonable SNR and number of antennas. Hence, in the following subsections, we propose different solutions in order to deal with the mentioned issues.

Regarding the limited number of antennas at the UE, we must find some other ways to perform the averaging, either in time or frequency domain, that bring us the SINR gain required for a good performance of the NCDS. This is particularly needed if we want to multiplex several UEs in the constellation domain, additionally to the spatial domain. We propose to exploit the frequency dimension instead of time due to the fact that we can independently process each OFDM symbol, and hence, we can reduce the overall latency as one of the requirements of 5G. Note that our proposed scheme can be easily extended to either time domain (processing several consecutive OFDM symbols) or spatial dimension at the receiver (increasing the number of antennas of the UE).

A. Frequency diversity

The frequency diversity can be exploited by transmitting the same differential complex symbol in K_d different subcarriers out of K. Based on the results of [27], we select the frequency

rather than a time domain scheme to reduce the delay as much as possible. Hence, the mapping of the DPSK sysmbols $\mathbf{r}_d^{mu}$ to the K subcarriers is as follows

$$\mathbf{s}_u^m = \sqrt{p_u}\left(\mathbf{1}_{K_d\times 1}\otimes \mathbf{r}_d^{mu}\right), \quad K_d A = K. \tag{18}$$

At the receiver, given (15), we must collect all $\left[\mathbf{y}_k^m\right]_u$ that come from the same transmitted complex symbol as

$$\breve{\mathbf{y}}_k^{mu} = \left[\left[\mathbf{y}_k^m\right]_u \quad \left[\mathbf{y}_{k+A}^m\right]_u \quad \cdots \quad \left[\mathbf{y}_{K_d-1}^m\right]_u\right]^T, \ 1\le k\le A, \tag{19}$$

where A is the number of transmitted symbols defined in (17), and it must be large enough in order to guarantee that the correlation among different subcarriers in $\breve{\mathbf{y}}_k^{mu}$ is as small as possible. Note that the correlation between any two subcarriers (k and $k+D$) can be defined as

$$\rho\left(D\right)\sigma_h^2 = \mathbb{E}\left\{\left(\breve{h}_k^{mu}\right)^* \breve{h}_{k+D}^{mu}\right\}, \quad \sigma_h^2 = \mathbb{E}\left\{\left|\breve{h}_k^{mu}\right|^2\right\}. \tag{20}$$

The received data from two contiguous subcarriers are non-coherently combined and averaged over several subcarriers that carry the same transmitted data as

$$z_a^{mu} = z_k^{mu} = \frac{1}{K_d}\left(\breve{\mathbf{y}}_k^{mu}\right)^H \breve{\mathbf{y}}_{k+1}^{mu}, \quad 1\le k\le A, \tag{21}$$

that can be expanded as

$$\begin{aligned} z_a^{mu} = {} & p_u\frac{\left[\mathbf{r}^{mu}\right]_a}{K_d}\sum_{k\in\mathcal{K}}\left(\breve{h}_k^{mu}\right)^*\breve{h}_{k+1}^{mu} + \\ & + \frac{1}{K_d}\sum_{k\in\mathcal{K}}\left(\left[\breve{\mathbf{w}}_k^m\right]_u\right)^*\left[\breve{\mathbf{w}}_{k+1}^m\right]_u + \\ & + \frac{\sqrt{p_u}}{K_d}\left(\left(\left[\mathbf{r}_d^{mu}\right]_a\right)^*\sum_{k\in\mathcal{K}}\left(\breve{h}_k^{mu}\right)^*\left[\breve{\mathbf{w}}_{k+1}^m\right]_u + \right. \\ & \left. + \left[\mathbf{r}_d^{mu}\right]_{a+1}\sum_{k\in\mathcal{K}}\left(\left[\breve{\mathbf{w}}_k^m\right]_u\right)^*\breve{h}_{k+1}^{mu}\right), \end{aligned} \tag{22}$$

where $\mathcal{K} = \{k, k+A, \ldots, k+A\left(K_d-1\right)\}$ is the set that contains all subcarrier indexes which are transmitting the same differential symbol. Making use of the Law of Large Numbers [42] and (20), we have that

$$z_a^{mu} \xrightarrow{K_d\to\infty} \rho\left(1\right)\sigma_h^2 p_u\left[\mathbf{r}^{mu}\right]_a, \tag{23}$$

where the self-interference, MUI and noise terms are averaged out by exploiting the frequency diversity.

Finally, given z_a^{mu}, the symbol decision is made by

$$\left[\widehat{\mathbf{r}}^{mu}\right]_a = \arg\min\left\{\left|\left[\widehat{\mathbf{r}}^{mu}\right]_a - z_a^{mu}\right|, \quad \left[\widehat{\mathbf{r}}^{mu}\right]_a \in C\right\}, \tag{24}$$

where C denotes the set that contains all the symbols of the PSK constellation used in the transmitter.

B. Determination of beams

In order to increase the number of simultaneously served UEs and be able to leverage the large number of antennas at the BS, we propose the integration of beam-forming with the NCDS, where the different beams will be capable of separating the UEs by their angular position. Furthermore, if there are several UEs that are very close to each other, an additional multiplexing method can be also implemented on top of it, such as time, frequency or constellation domain. As we mentioned before, our technique relies on the beam-management procedure [20] where the BS selects one azimuth angle for each UE ($\widehat{\theta}^u$, $u = 1, \ldots, U$).

Once the angles are chosen, we adopt the conventional beam-forming [43], which is a spatial filter capable of focusing the transmitted power of the BS towards these angles, where $\mathbf{b}_u$ is given by

$$\mathbf{b}_u = \mathbf{a}^*\left(\widehat{\theta}^u\right), \quad 1\le u\le U. \tag{25}$$

Note that our proposed NCDS can be combined with any beam-forming technique. We choose this very simple linear scheme because in combination with the beam-management procedure of 5G it has a very reduced overhead. It allows us to exemplify our proposal with reduced complexity, which also has an impact on the system latency.

Hence, (16) can be rewritten as

$$\sigma_{i^u}^2 = \sum_{\substack{u'=1\\u'\neq u}}^{U} p_{u'}\sum_{c=1}^{C}\frac{\sigma_c^2}{R}\sum_{r=1}^{R}\left(\frac{\sin\left(\frac{V}{2}\times l\left(\theta^u,\theta^{u'}\right)\right)}{\sin\left(\frac{l\left(\theta^u,\theta^{u'}\right)}{2}\right)}\right)^2, \tag{26}$$

due to the fact that

$$\begin{aligned} \mathbf{a}_u^H\mathbf{a}_{u'} = {} & \sum_{v=0}^{V-1} e^{-jv\times l\left(\theta^u,\theta^{u'}\right)} = \\ = {} & \left\{\begin{array}{ll} 1 & u=u' \\ e^{-j\frac{V-1}{2}\times l\left(\theta^u,\theta^{u'}\right)}\frac{\sin\left(\frac{V}{2}\times l\left(\theta^u,\theta^{u'}\right)\right)}{\sin\left(\frac{l\left(\theta^u,\theta^{u'}\right)}{2}\right)} & u\neq u' \end{array}\right\}, \end{aligned} \tag{27}$$

where $l\left(\theta^u,\theta^{u'}\right) = \frac{2\pi d}{\lambda}\Delta$ and $\Delta = \cos\left(\theta^u\right) - \cos\left(\theta^{u'}\right)$. Note that (27) corresponds to the well-known "sinc" function.

Ideally, if we want to completely remove the MUI component, we must find the zeros of the "sinc" function which correspond to those angles that satisfy that

$$\frac{2\pi d}{\lambda}\Delta = \frac{2\pi}{V}v \implies \Delta = v\frac{\lambda}{Vd}, \quad 0\le v\le V-1. \tag{28}$$

However, in realistic scenarios, it is almost impossible to completely remove the MUI due to the fact that the signal that arrives to each UE comes from many clusters which are randomly placed around it. Hence, in order to also keep the MUI low without decreasing p_u, the BS has to select only those UEs with a certain angular distance (large Δ). We show some illustrative performance in Section VI that may help design the scheduler, which is out of the scope of the present work.

IV. Analysis of the SINR

For a realistic scenario, when K_d is not large enough for (23) to hold, the different undesirable interference and noise terms in (22) are not mitigated. We can characterize the power of these undesirable components as

$$\mathbb{E}\left\{\left|\rho\left(1\right)\sigma_h^2 p_u\left[\mathbf{r}^{mu}\right]_a - z_a^{mu}\right|^2\right\} = \sum_{i=1}^{4}\mathbb{E}\left\{\left|g_i\right|^2\right\}, \tag{29}$$

where (29) can be expressed as the sum of four independent terms due to the fact that the joint MUI and noise, the multi-path channel and the transmitted symbols are independent to each other. Following a similar procedure to [23] and [27], each term is given by

$$\mathbb{E}\left\{|g_1|^2\right\} = \mathbb{E}\left\{\left|\frac{1}{K_d}\sum_{k\in\mathcal{K}}\left(\left[\check{\mathbf{w}}_k^m\right]_u\right)^*\left[\check{\mathbf{w}}_{k+1}^m\right]_u\right|^2\right\} = \frac{\sigma_{\check{w}}^4}{K_d}, \quad (30)$$

$$\mathbb{E}\left\{|g_2|^2\right\} = \mathbb{E}\left\{|g_3|^2\right\} = \\ = \mathbb{E}\left\{\left|\sqrt{p_u}\frac{\left(\left[\mathbf{r}_d^{mu}\right]_a\right)^*}{K_d}\sum_{k\in\mathcal{K}}\left(\check{h}_k^{mu}\right)^*\left[\check{\mathbf{w}}_{k+1}^m\right]_u\right|^2\right\} = \frac{\sigma_{\check{w}}^2\sigma_h^2 p_u}{K_d}, \quad (31)$$

$$\mathbb{E}\left\{|g_4|^2\right\} = \\ = \mathbb{E}\left\{\left|p_u\left[\mathbf{r}^{mu}\right]_a\left(\rho\left(1\right)\sigma_h^2 - \frac{1}{K_d}\sum_{k\in\mathcal{K}}\left(\check{h}_k^{mu}\right)^*\check{h}_{k+1}^{mu}\right)\right|^2\right\} = \\ = p_u^2\sigma_h^4\left(\frac{1}{K_d} + \frac{1}{K_d^2}\sum_{k_1\in\mathcal{K}}\sum_{\substack{k_2\in\mathcal{K}\\k_1\neq k_2}}\rho^2\left(|k_2-k_1|\right)\right), \quad (32)$$

where (30) accounts for the power of the product of the noise terms, (31) denotes the cross product terms between the noise and signal, and (32) is the power of the signal product which confirms that the correlation among subcarriers that carry the same complex symbol must be as low as possible in order to constrain the self-interference, as we stated in (20). Moreover, when $\rho\left(|k_2-k_1|\right)=0$, (32) has the same expression shown in [23] for the single-user (SU) case and frequency-flat channel.

Therefore, making use of (23) and (30)-(32), the SINR for any single antenna UE can be shown to be given by

$$\text{SINR} = \frac{\rho^2\left(1\right)K_d}{1+\frac{1}{K_d}\sum_{k_1\in\mathcal{K}}\sum_{\substack{k_2\in\mathcal{K}\\k_1\neq k_2}}\rho^2\left(|k_2-k_1|\right)+\frac{\sigma_{\check{w}}^4}{p_u^2\sigma_h^4}+2\frac{\sigma_{\check{w}}^2}{p_u\sigma_h^2}}, \quad (33)$$

where $\rho\left(1\right)$ is pointing out that the two contiguous (in frequency) differential symbols must experience the same channel response, or as similar as possible, in order to perform the differential modulation scheme. The averaging factor K_d not only linearly increases the SINR, but it also attenuates the correlation among those subcarriers to be averaged (second term of the denominator). Note that the effect of using beam-forming is implicit in (33). On one hand, the MUI given by $\sigma_{\check{w}}^2$ is reduced by rejecting the signals coming from the clusters of other UEs through the spatial separation provided by the beam-forming, see (26). On the other hand, the beam-forming will also enhance the power gain of the UE of interest (σ_h^2), which is given by (15) and (20). Hence, we can see that the performance of the system strongly depends on the noise and MUI effects ($\sigma_{\check{w}}^2$), which may increase the third and fourth term in the denominator. Furthermore, due to the fact that the diversity is being exploited in the frequency dimension, it is crucial that the different subcarriers carrying the same information should be as much uncorrelated as possible ($\rho^2\left(|k_2-k_1|\right) << 1$), in order to leverage the desired diversity. Otherwise, an additional degradation will appear as shown in the second term of the denominator.

V. Complexity analysis

In order to show the validity of our proposal, we perform a complexity comparison between the proposed NCDS and the CDS based on ZF or MRT. In order to provide a fair comparison, the complexity analysis is done assuming that all these three techniques are combined with beam-forming (the complexity of a complete ZF or MRT with the V antennas would be much higher). The comparison is done in terms of the number of required real multiplications (NRM). The additional complexity introduced by the beam-forming is not taken into account due to the fact that it is the same for all the three techniques.

The NRM for the NCDS is given by

$$\begin{aligned}\text{NRM}_{NCDS} &= 3M\left(A-1\right)+3MK_d\left(A-1\right) = \\ &= 3M\left(A-1\right)+3M\left(K-K_d\right),\end{aligned} \quad (34)$$

where the two terms represent the differential encoding at the BS and decoding at UE processes of the differential modulation scheme, and the factor 3 comes from assuming that one complex multiplication implies three real multiplications.

The NRM for the MRT technique is given by

$$\begin{aligned}\text{NRM}_{MRT} &= 2K_pM_p+\left(K_p-1\right)\left(M_p-1\right)+ \\ &+3\left(KM-K_pM_p\right),\end{aligned} \quad (35)$$

where the three terms represent the channel estimation, interpolation and equalization processes, respectively. In this equation, K_p and M_p denote the number of pilots placed in the frequency and time domain, respectively, for M consecutive OFDM symbols. Note that (35) does not depend on the parameter V due to the fact that the massive number of antennas is used for beam-forming and not accounted for the complexity comparison. In the case of ZF, its NRM is the same as for MRT with an additional term that accounts for the computation of the equalizer by a matrix inversion, so the expression is given by

$$\begin{aligned}\text{NRM}_{ZF} &= 2K_pM_p+\left(K_p-1\right)\left(M_p-1\right)+ \\ &+6\left(KM-K_pM_p\right).\end{aligned} \quad (36)$$

Comparing (34) with (35) and (36), the dominant term of each expression corresponds to the last one which depends on both M and K. Therefore, our proposed NCDS has a similar complexity to MRT ($O\left(3KM\right)$) and half of ZF ($O\left(6KM\right)$). In the next section, we will provide some simulation results in order to show that our proposed NCDS is the scheme with the best trade-off in terms of complexity and performance.

Moreover, any of the CDS requires much more memory storage than the NCDS due to the fact that the estimated channels and equalizers for each time-frequency-space resource must be stored. The read/write operations of the memory also require a significant time, which will increase the latency of the system.

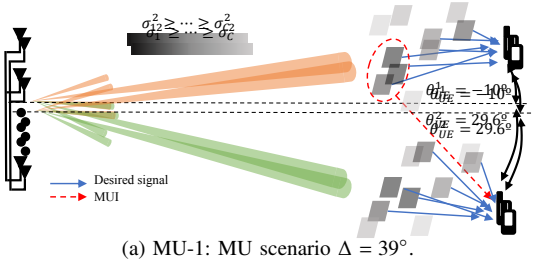

(a) MU-1: MU scenario $\Delta = 39°$.

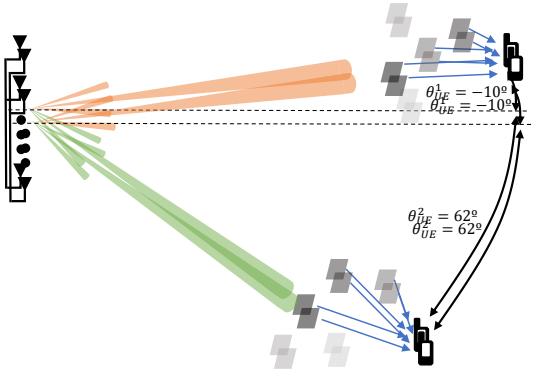

(b) MU-2: MU scenario $\Delta = 72°$.

Fig. 2. Two examples of MU scenarios.

TABLE II
SIMULATION PARAMETERS

K	4096	**Constellation**	16-PSK
Δf	30 KHz	**K_d**	32
AS	5° & 10°	**DS**	16 & 363 ns
V	64	**U**	2
M	14	**Power delay profile**	CDL-B

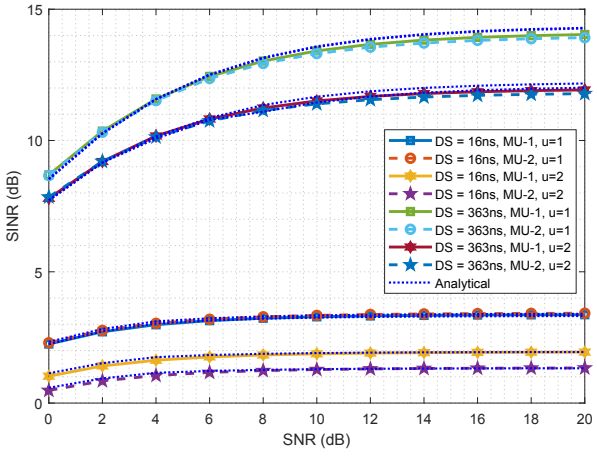

Fig. 3. Theoretical and simulated SINR.

VI. Numerical Results

In this section, we provide some numerical results to analyse the performance of our proposed scheme and validate the obtained analytical expressions.

A. Scenarios and parameters

Due to the fact that the angular position of all UEs is crucial in order to keep the MUI low, we set two illustrative cases of MU scenarios (MU-1 and MU-2) described in Fig. 2. In the scenario shown in Fig. 2a, some strong clusters of UE1 will interfere to UE2 through the side lobes of the array. Additionally, we also provide the numerical results for the SU scenarios for each UE as a benchmark, where SU-1 and SU-2 correspond to UE1 and UE2 transmitting in isolation, respectively.

In Table II, we can see the default numerical values for the parameters that we defined in the previous sections, where Δf represents the subcarrier spacing, AS and DS denote the angular and delay spread of the channel, respectively. The parameters that define the numerology of the waveform are taken from 5G NR [1], and the parameters related to the channel model [39], [40] are examples provided by 3GPP for a wide range of the spectrum, from 2 GHz up to 70 GHz, given in [44]. The SNR is defined as

$$\text{SNR} = \frac{\left\|\mathbf{y}_k^{mu}\right\|_F^2}{V\sigma_w^2}. \tag{37}$$

For the sake of conciseness, we assume that all UEs have the same allocated power ($p_u = 0.5, \ \forall u$), and we also assume that the selected angle $\widehat{\theta}^u$ for the design of $\mathbf{b}_u$ corresponds to the angle of that cluster whose gain is the maximum one for the u-th UE.

B. Complexity comparison

In Table III, we provide the NRM for our proposed NCDS against different CDS. Only for the particular case of CDS, we set M_p and K_p according to [1]. We can see that the NRM of ZF is almost twice the number of our proposed scheme, while for MRT it is just slightly lower. Additionally, all numerical NRM values are upper-bounded by the complexity order provided in the previous section, showing that the parameters K and M are the dominant ones. Even though less complex, it is well-known that MRT has generally a much worse performance than ZF, which is outperformed by NCDS as we will show in the next subsections.

C. Verification of the SINR expression

In Fig. 3, we show the comparison between the SINR given by the analytical expression and the simulation results, where we can see that our analysis is accurate for different scenarios. We can see that our proposal works better in frequency-selective channels (DS = 363 ns), where the low correlation among different subcarriers helps to reduce the MUI and noise effects as we expected, giving a higher SINR. The UE1 outperforms UE2 due to the fact that several strong clusters of the former are interfering to the latter, as we also mentioned before. Once validated, the provided SINR expressions can be used for the system design, to evaluate important parameters such as the energy efficiency (EE), and to develop scheduling algorithms.

D. Energy efficiency (EE)

Similarly to [11], [12], the EE is defined as

$$\text{EE} = \frac{\log_2\left(1+\text{SINR}\right)}{\text{SNR}\times\sigma_w^2\times 10^9}\left[\frac{\text{Mbps}}{\text{Hz}\times\text{mW}}\right], \tag{38}$$

TABLE III
COMPLEXITY COMPARISON

	NCDS		ZF		MRT	
	$K_p = \frac{K}{2}$	$K_p = \frac{K}{3}$	$K_p = \frac{K}{2}$	$K_p = \frac{K}{3}$	$K_p = \frac{K}{2}$	$K_p = \frac{K}{3}$
$M_p = 1$	167958	167958	335872	338604	169984	170667
$M_p = 2$	167958	167958	329727	334508	169983	170666
$M_p = 3$	167958	167958	323582	330412	169982	170665
$M_p = 4$	167958	167958	317437	326316	169981	170664
Complexity order	**172032**		**344064**		**172032**	

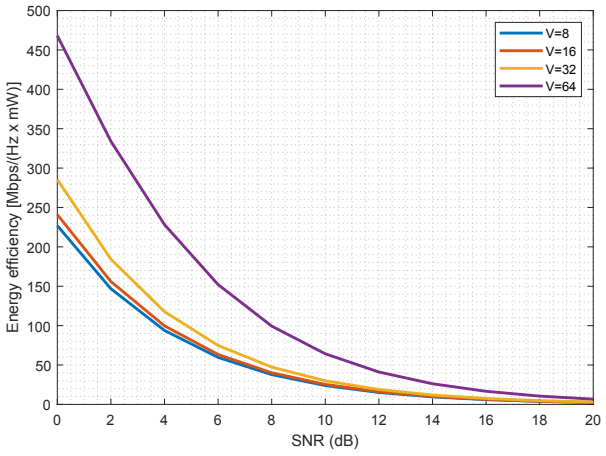

Fig. 4. Variation of the energy efficiency with the number of antennas.

where 10^9 accounts for the conversion from bps to Mbps and W to mW, and SINR is given by expression (33). In Fig. 4, we show the EE of the NCDS by using different number of antennas of the BS for the UE2 under the scenario of MU-2 when $DS = 363$ ns, $AS = 5°$ and $\sigma_w^2 = -80$ dBm. We can see that a higher number of antenna elements at the BS will improve the efficiency of the overall system, showing that our proposed scheme can take advantage of the massive MIMO, unlike the other existing non-coherent techniques in the literature. For example, increasing the number of antennas from $V = 32$ to $V = 64$ corresponds to almost doubling the EE.

E. Error probability for CDS and NCDS with conventional beam-forming

In order to show the effectiveness of our proposal, we compare it with the CDS based only in ZF due to the fact that MRT is known to have a worse performance than ZF. We choose $K_p = K/2$ and $M_p = 4$ according to [1]. In order to provide a fair comparison in terms of performance and rate, CDS is not only implemented with the conventional beam-forming, but also frequency diversity is included, where an averaging process over several subcarriers is done before the symbol decision, identical to the one in NCDS.

Besides, as shown in [27], an additional phase estimation and compensation is required when combining NCDS and OFDM. In particular, it is very important for strongly frequency-selective channels, where the additional phase is very noticeable. Similarly to [27], we define several cases for the phase estimation, such as the perfect estimation (PE) case as a benchmark, non-estimation (NE), where the additional phase estimation and correction methods are not used; and a realistic estimation (RE) case where only two pilots are used for the phase estimation for M consecutive OFDM symbols.

In Figs. 5a and 5b, we plot the performance of both UEs for $DS = 16$ ns and $AS = 5°$. In Fig. 5a (UE1), our technique significantly outperforms CDS due to the fact that there is enough angular separation between the two UEs (MU-2). When the angular spacing is reduced (MU-1), our proposal is degraded due to the MUI caused by UE2, and the difference between NCDS and CDS is reduced but still quite noticeable. In Fig. 5b (UE2), we can see that the performance of the second UE is worse than the first one due to the strong MUI caused by the latter in the particular scenario that we are analysing. In MU-2 scenario, even though the performance is worse, it keeps being much better than with CDS. However, when the angular space is not large enough (MU-1), NCDS only slightly outperforms CDS. Note that we are facing an almost flat-fading channel, and as stated in (33), there is not enough frequency-selectivity in order to reduce the MUI and noise effects, especially for MU-1 scenario. Furthermore, both PE and NE cases have the same performance, due to the reduced number of taps of the channel, where the phase difference of any two contiguous subcarriers is negligible, as also shown in [27], rendering the phase correction unnecessary.

In Fig. 5c and 5d, we provide the performance of both UEs for $DS = 363$ ns and $AS = 5°$. Comparing these two figures with the two previous ones, we can see that the performance of our technique in frequency-selective channels is much better, thanks to the low correlation among subcarriers which is capable of effectively mitigating the effects of MUI and noise. For UE1, no matter in which MU scenario we are, both curves show the same performance and it is almost the same as compared to its corresponding SU case. For UE2, MU-2 and SU-2 scenarios have almost the same performance, which is much better than for the case of MU-1. Furthermore, we can also see that the additional phase compensation is a must for this kind of channels in order to have an acceptable performance, while it is not important for the not very frequency-selective channels. We can see that the performance for the case of RE (with only two additional pilots for the phase estimation) is only slightly worse than the ideal case of PE.

In Figs. 5e and 5f, we show the performance of both UEs for $DS = 363$ ns and $AS = 10°$. Comparing again these two figures with the two previous ones where the AS was lower, we can see that the performance of both UEs is worse due to the increment of the AS, which corresponds to an enhancement of the MUI. NCDS of UE1 keeps outperforming the CDS for both cases of angular separation. However, the performance of UE2 only keeps being clearly better than CDS for the

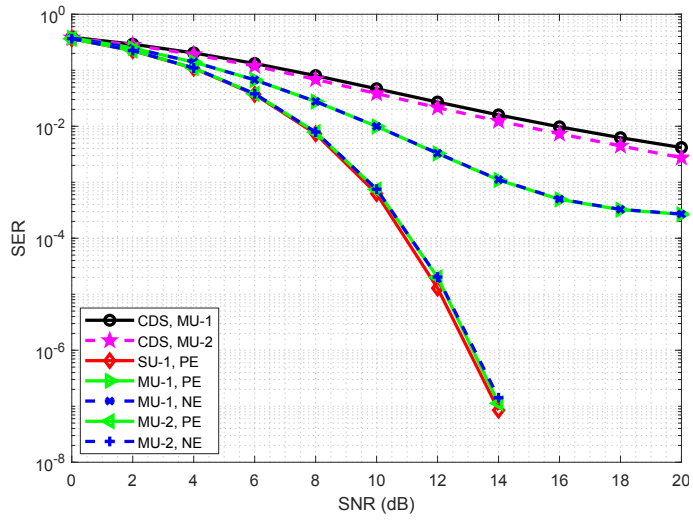

(a) UE1 for DS = 16 and AS = 5°.

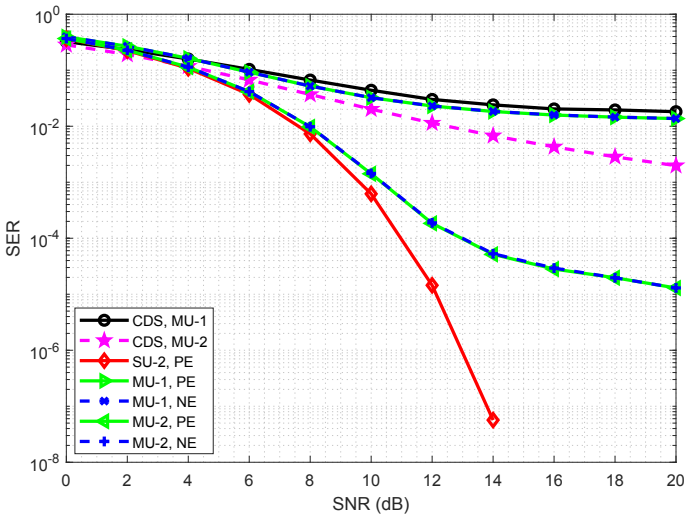

(b) UE2 for DS = 16 ns and AS = 5°.

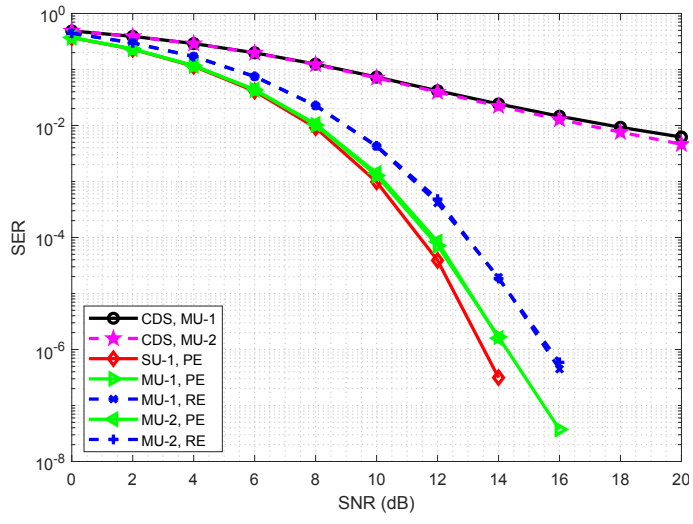

(c) UE1 for DS = 363 ns and AS = 5°.

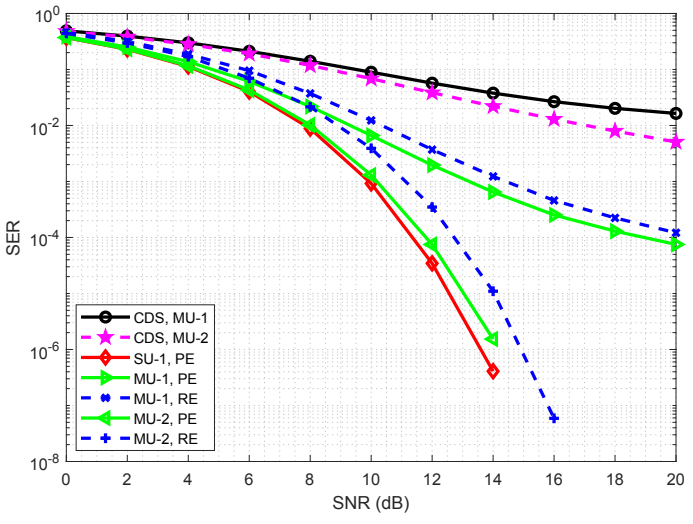

(d) UE2 for DS = 363 ns and AS = 5°.

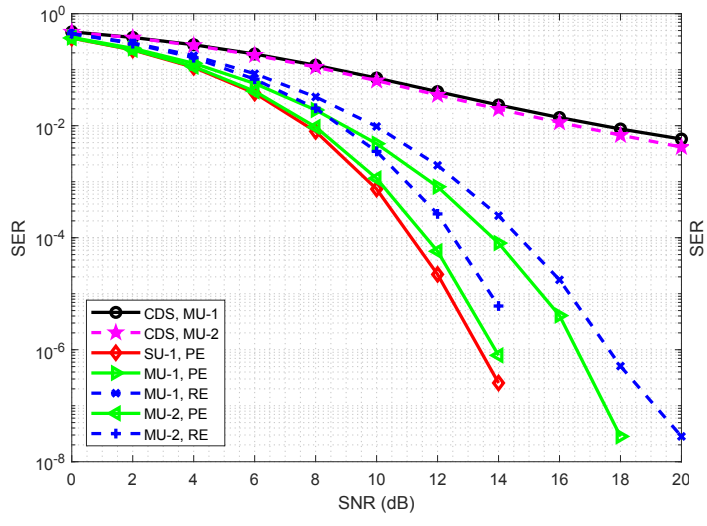

(e) UE1 for DS = 363 ns and AS = 10°.

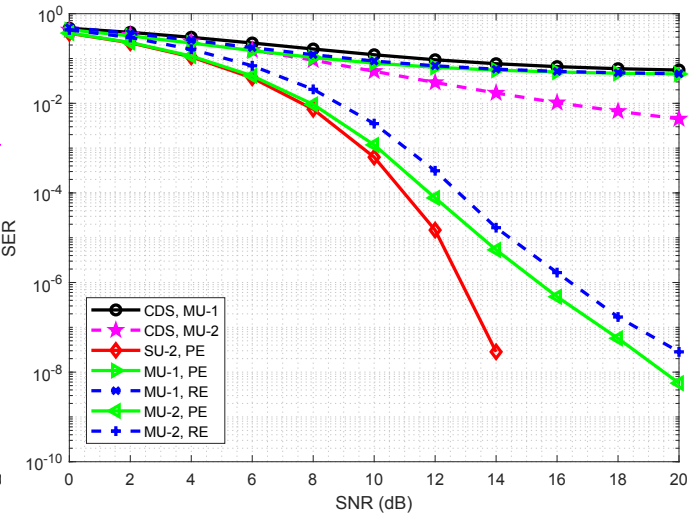

(f) UE2 for DS = 363 ns and AS = 10°.

Fig. 5. SER comparison for conventional beam-forming in different scenarios.

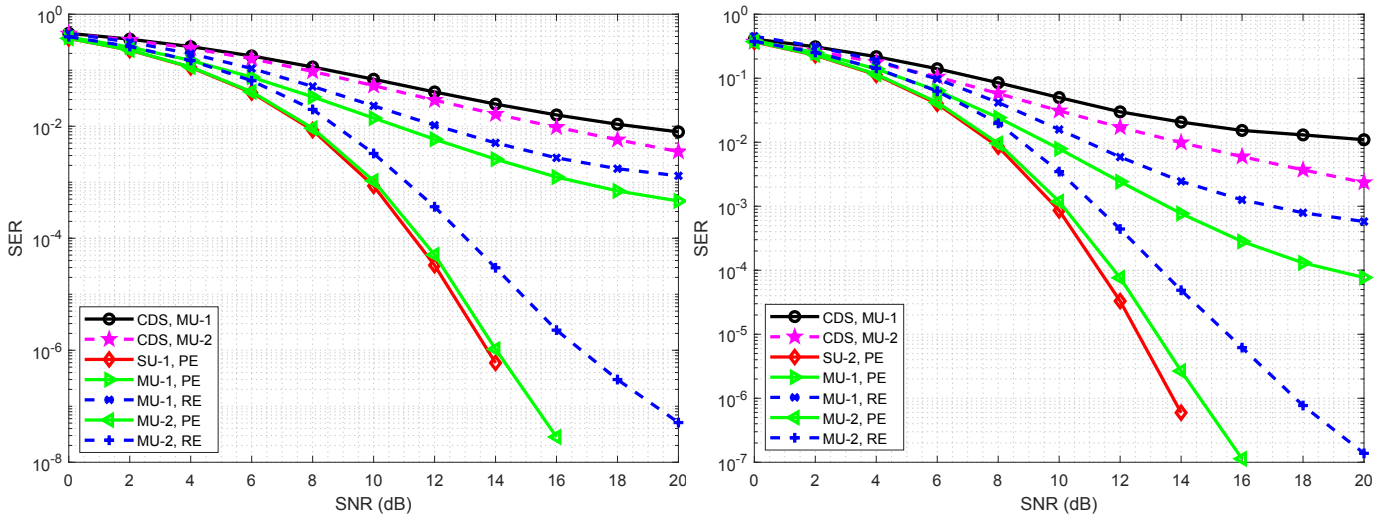

(a) UE1 (b) UE2

Fig. 6. SER comparison for precoding based on PMI type I in the scenario of $DS = 363$ ns, $AS = 5°$.

particular case of MU-2, while it is only slightly better than CDS for the case of MUI-1.

F. Error probability for CDS and NCDS with precoding based on PMI type I

In order to show the flexibility of our proposal, we also implement our proposed NCDS with one of the precoding techniques defined by the 5G NR [1], namely precoding based on a precoding matrix indicator (PMI). In Figs. 6a and 6b, we plot the performance of both UEs for $DS = 363$ ns and $AS = 5°$ when the precoding based on PMI type I is used. We can see that our proposal keeps outperforming CDS (where the same precoding is used combined with ZF) for different scenarios. We show that our proposal can be adaptable to different precoding schemes, including this kind of codebook based techniques.

G. Analysis of the throughput

Using the same previously defined parameters, we provide the effective throughput of each scheme which is defined as

$$T_r = \begin{cases} \eta N_B \left(1 - \text{SER}\right) \text{BW}, & \text{SER} \geq \text{SER}_{th} \\ 0, & \text{otherwise} \end{cases}, \tag{39}$$

where BW corresponds to the band-width of the signal measured in Hz, η is the efficiency measured as the effective number of transmitted data symbols on M consecutive OFDM symbols (to account for the inefficiency of reference signals, when included, and the frequency averaging process), N_B denotes the number of bits per symbol in the constellation and SER_{th} represents a SER threshold imposed by some criteria. According to the literature, this threshold can be constrained by the block error rate (BLER) as

$$\text{BLER} = 1 - \left(1 - \text{SER}\right)^L. \tag{40}$$

where L denotes the length of the data block. Typically, if the BLER is higher than 10%, the whole block is discarded. Assuming that BW = 100 MHz, the throughput T_r is measured in mega bits per second (Mbps).

If Figs. 7a and 7b , we show a throughput comparison of UE2 (to show the worst case) when the conventional beamforming is adopted, for RE case, $DS = 363$ ns, $AS = 5°$ and $\text{SER}_{th} = 10^{-2}$. In Fig. 7a, we compare the throughput of CDS and NCDS for 16-PSK, where the latter not only has a higher throughput due to the absence of any reference signal, but it also works for moderate values of SNR. In Fig. 7b, we plot the throughput of NCDS under the scenario of MU-2 for different number of antennas (V) and different modulation schemes. We can see that depending on the value of the SNR, higher order constellations can be selected to provide a greater throughput. Moreover, a large number of antennas ($V = 64$) will provide narrower beams which are capable of efficiently multiplexing the different UEs in the spatial domain and at the same time reducing the MUI. For the case of MU-2, increasing the number of antennas from $V = 8$ to $V = 64$ will provide a significant improvement, where an array of eight elements is not enough to spatially separate both UEs. However, from $V = 32$ to $V = 64$ the improvement is only slight due to the fact that the angular distance of the two UEs is already high and the beam produced by an array of 32 elements is narrow enough.

H. SNR gain

The SNR gain is computed in dB as

$$\gamma\left(\text{SER}_{th}\right) = \left|\text{SNR}_{ref}\left(\text{SER}_{th}\right) - \text{SNR}\left(\text{SER}_{th}\right)\right|, \tag{41}$$

where $\text{SNR}\left(\text{SER}_{th}\right)$ corresponds to the minimum required SNR in order to achieve SER_{th}.

In Table IV, we provide the SNR gain of NCDS by using different number of antennas and different modulations of UE2 under the scenario of MU-2 for RE case, $DS = 363$ ns, $AS = 5°$ and we set the case of $V = 8$ as the reference one. We can see that when the number of array elements is increased, the

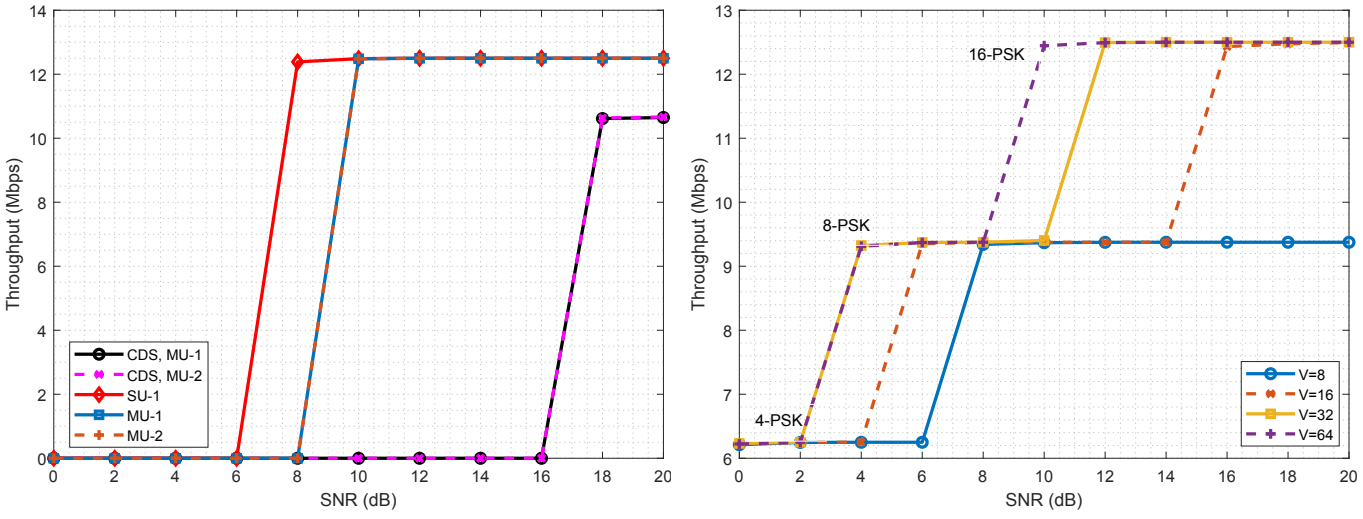

(a) CDS vs NCDS for 16-PSK.

(b) Different values of V and modulation schemes for MU-2.

Fig. 7. Throughput comparison of UE2 for RE case, DS = 363 ns, $AS = 5°$ and $\text{SER}_{th} = 10^{-2}$.

TABLE IV
SNR GAIN (SETTING $V = 8$ AS THE REFERENCE CASE)

	4-PSK $\text{SER}_{th} = 10^{-5}$	8-PSK $\text{SER}_{th} = 10^{-5}$	16-PSK $\text{SER}_{th} = 10^{-2}$
$V = 16$	0.8 dB	3.5 dB	12.8 dB
$V = 32$	1.1 dB	5.5 dB	17.1 dB
$V = 64$	1.3 dB	5.8 dB	17.4 dB

efficiency of the system is also increased for all modulation schemes. This SNR gain increase is more significant for higher order constellations, where the high number of antennas is crucial in order to keep the interference and noise terms as low as possible.

VII. CONCLUSIONS

In this paper we have proposed a novel NCDS combined with beam-forming for the DL of a MIMO-OFDM system, applicable to an evolution of the 5G NR for different scenarios, for both sub-6 GHz and mm-Waves bands. The use of a beam-forming technique is chosen in order to work in a MU scenario, where different UEs are multiplexed in the space domain, leveraging a large number of antennas at the BS (massive MIMO). The frequency diversity is also leveraged in order to enable the integration of the differential modulation scheme in the DL, where UEs are constrained to be equipped with a small number of antennas (single antenna in this work).

We have provided some analytical expressions of the SINR that are shown to match the numerical results, where the close form expressions can be used to design some scheduling algorithms or for the system design. We have also provided a comparison of the complexity in terms of NRM showing that our proposal offers a much better performance-complexity trade-off than ZF and MRT CDS alternatives. Through the numerical results based on SER, throughput, SNR gain and EE, we validated our proposed scheme outperforms the traditional CDS with a higher throughput, for several representative scenarios with different spatial and frequency-selectivity conditions. Our proposed scheme can obtain between 20% and 50% additional throughput for high and moderate values of SNR, respectively, with half the complexity as compared to the traditional ZF. The use of the developed SINR expressions for scheduling or user grouping is an interesting topic for further work.

REFERENCES

[1] *Physical channels and modulation (Release 15)*, 3GPP Std. 38.211, 2018.

[2] A. Ghosh, A. Maeder, M. Baker, and D. Chandramouli, "5G Evolution: A view on 5G cellular technology beyond 3GPP Release 15," *IEEE Access*, vol. 7, pp. 127 639–127 651, 2019.

[3] R. Vannithamby and S. Talwar, *Towards 5G: Applications, Requirements and Candidate Technologies*, 1st ed. Wiley, 2007.

[4] E. G. Larsson, O. Edfors, F. Tufvesson, and T. L. Marzetta, "Massive MIMO for next generation wireless systems," *IEEE Communications Magazine*, vol. 52, no. 2, pp. 186–195, Feb. 2014.

[5] T. Hwang, C. Yang, G. Wu, S. Li, and G. Y. Li, "OFDM and its wireless applications: A survey," *IEEE Transactions on Vehicular Technology*, vol. 58, no. 4, pp. 1673–1694, May 2009.

[6] W. Huang, Y. Huang, R. Zhao, S. He, and L. Yang, "Wideband millimeter wave communication: Single carrier based hybrid precoding with sparse optimization," *IEEE Transactions on Vehicular Technology*, vol. 67, no. 10, pp. 9696–9710, Oct. 2018.

[7] J. Lota, S. Sun, T. S. Rappaport, and A. Demosthenous, "5G uniform linear arrays with beamforming and spatial multiplexing at 28, 37, 64, and 71 ghz for outdoor urban communication: A two-level approach," *IEEE Transactions on Vehicular Technology*, vol. 66, no. 11, pp. 9972–9985, Nov. 2017.

[8] B. Yang, Z. Yu, J. Lan, R. Zhang, J. Zhou, and W. Hong, "Digital beamforming-based massive MIMO transceiver for 5G millimeter-wave communications," *IEEE Transactions on Microwave Theory and Techniques*, vol. 66, no. 7, pp. 3403–3418, July 2018.

[9] R. Zhang, J. Zhou, J. Lan, B. Yang, and Z. Yu, "A high-precision hybrid analog and digital beamforming transceiver system for 5g millimeter-wave communication," *IEEE Access*, vol. 7, pp. 83 012–83 023, 2019.

[10] Y. Xu, X. Shi, W. Li, J. Xu, and L. Huang, "Low-sidelobe range-angle beamforming with FDA using multiple parameter optimization," *IEEE Transactions on Aerospace and Electronic Systems*, vol. 55, no. 5, pp. 2214–2225, Oct. 2019.

[11] A. Kaushik, E. Vlachos, C. Tsinos, J. Thompson, and S. Chatzinotas, "Joint bit allocation and hybrid beamforming optimization for energy efficient millimeter wave MIMO systems," arXiv:1909.12170, 2019.

[12] A. Kaushik, J. Thompson, E. Vlachos, C. Tsinos, and S. Chatzinotas, "Dynamic RF chain selection for energy efficient and low complexity hybrid beamforming in millimeter wave MIMO systems," *IEEE Transactions on Green Communications and Networking*, vol. 3, no. 4, pp. 886–900, Dec. 2019.

[13] X. Gao, O. Edfors, F. Tufvesson, and E. G. Larsson, "Massive MIMO in real propagation environments: Do all antennas contribute equally?" *IEEE Transactions on Communications*, vol. 63, no. 11, pp. 3917–3928, Nov. 2015.

[14] X. Ma, F. Yang, S. Liu, J. Song, and Z. Han, "Sparse channel estimation for MIMO-OFDM systems in high-mobility situations," *IEEE Transactions on Vehicular Technology*, vol. 67, no. 7, pp. 6113–6124, July 2018.

[15] C. Chen and W. Wu, "Joint AoD, AoA, and channel estimation for MIMO-OFDM systems," *IEEE Transactions on Vehicular Technology*, vol. 67, no. 7, pp. 5806–5820, July 2018.

[16] A. Kaushik, E. Vlachos, J. Thompson, and A. Perelli, "Efficient channel estimation in millimeter wave hybrid MIMO systems with low resolution ADCs," in *2018 26th European Signal Processing Conference (EUSIPCO)*, Sep. 2018, pp. 1825–1829.

[17] J. Flordelis, F. Rusek, F. Tufvesson, E. G. Larsson, and O. Edfors, "Massive MIMO performance - TDD versus FDD: What do measurements say?" *IEEE Transactions on Wireless Communications*, vol. 17, no. 4, pp. 2247–2261, April 2018.

[18] J. Vieira, F. Rusek, O. Edfors, S. Malkowsky, L. Liu, and F. Tufvesson, "Reciprocity calibration for massive MIMO: Proposal, modeling, and validation," *IEEE Transactions on Wireless Communications*, vol. 16, no. 5, pp. 3042–3056, May 2017.

[19] H. Prabhu, J. Rodrigues, O. Edfors, and F. Rusek, "Approximative matrix inverse computations for very-large MIMO and applications to linear pre-coding systems," in *2013 IEEE Wireless Communications and Networking Conference (WCNC)*, April 2013, pp. 2710–2715.

[20] *Study on New Radio Access Technology Physical Layer Aspects (Release 14)*, 3GPP Std. 38.800, 2017.

[21] A. Manolakos, M. Chowdhury, and A. J. Goldsmith, "CSI is not needed for optimal scaling in multiuser massive SIMO systems," in *2014 IEEE International Symposium on Information Theory*, June 2014, pp. 3117–3121.

[22] T. V. Luong, N. A. V. Y. Ko, M. Matthaiou, and H. Q. Ngo, "Deep energy autoencoder for noncoherent multicarrier MU-SIMO systems," *IEEE Transactions on Wireless Communications*, 2020.

[23] A. G. Armada and L. Hanzo, "A non-coherent multi-user large scale SIMO system relaying on M-ary DPSK," in *2015 IEEE International Conference on Communications (ICC)*, June 2015, pp. 2517–2522.

[24] V. M. Baeza, A. G. Armada, M. El-Hajjar, and L. Hanzo, "Performance of a non-coherent massive SIMO M-DPSK system," in *2017 IEEE 86th Vehicular Technology Conference (VTC-Fall)*, Sept. 2017, pp. 1–5.

[25] V. M. Baeza, A. G. Armada, W. Zhang, M. El-Hajjar, and L. Hanzo, "A non-coherent multiuser large-scale SIMO system relying on M-ary DPSK and BICM-ID," *IEEE Transactions on Vehicular Technology*, vol. 67, no. 2, pp. 1809–1814, Feb. 2018.

[26] V. M. Baeza and A. G. Armada, "Non-coherent massive SIMO system based on M-DPSK for Rician channels," *IEEE Transactions on Vehicular Technology*, vol. 68, no. 3, pp. 2413–2426, March 2019.

[27] K. Chen-Hu and A. G. Armada, "Non-coherent multiuser massive MIMO-OFDM with differential modulation," in *2019 IEEE International Conference on Communications (ICC)*, May 2019.

[28] S. Li, J. Zhang, and X. Mu, "Design of optimal constellation for massive SIMO systems with riemannian distance," in *GLOBECOM 2017 - 2017 IEEE Global Communications Conference*, Dec. 2017, pp. 1–6.

[29] B. M. Hochwald and W. Sweldens, "Differential unitary space-time modulation," *IEEE Transactions on Communications*, vol. 48, no. 12, pp. 2041–2052, Dec. 2000.

[30] V. Tarokh and H. Jafarkhani, "A differential detection scheme for transmit diversity," *IEEE Journal on Selected Areas in Communications*, vol. 18, no. 7, pp. 1169–1174, July 2000.

[31] M. Beko, J. Xavier, and V. A. N. Barroso, "Noncoherent communication in multiple-antenna systems: Receiver design and codebook construction," *IEEE Transactions on Signal Processing*, vol. 55, no. 12, pp. 5703–5715, Dec. 2007.

[32] R. H. Gohary and T. N. Davidson, "Noncoherent MIMO communication: Grassmannian constellations and efficient detection," *IEEE Transactions on Information Theory*, vol. 55, no. 3, pp. 1176–1205, March 2009.

[33] A. Paulraj, R. Nabar, and D. Gore, *Introduction to Space-Time Wireless Communications*, 1st ed. New York, NY, USA: Cambridge University Press, 2008.

[34] J. Cabrejas, S. Roger, D. Calabuig, Y. M. M. Fouad, R. H. Gohary, J. F. Monserrat, and H. Yanikomeroglu, "Non-coherent open-loop MIMO communications over temporally-correlated channels," *IEEE Access*, vol. 4, pp. 6161–6170, 2016.

[35] M. Shafi, J. Zhang, H. Tataria, A. F. Molisch, S. Sun, T. S. Rappaport, F. Tufvesson, S. Wu, and K. Kitao, "Microwave vs. millimeter-wave propagation channels: Key differences and impact on 5G cellular systems," *IEEE Communications Magazine*, vol. 56, no. 12, pp. 14–20, Dec. 2018.

[36] C. Gustafson, K. Haneda, S. Wyne, and F. Tufvesson, "On mm-wave multipath clustering and channel modeling," *IEEE Transactions on Antennas and Propagation*, vol. 62, no. 3, pp. 1445–1455, March 2014.

[37] M. R. Akdeniz, Y. Liu, M. K. Samimi, S. Sun, S. Rangan, T. S. Rappaport, and E. Erkip, "Millimeter wave channel modeling and cellular capacity evaluation," *IEEE Journal on Selected Areas in Communications*, vol. 32, no. 6, pp. 1164–1179, June 2014.

[38] R. Hamdi, E. Driouch, and W. Ajib, "New efficient transmission technique for hetnets with massive MIMO wireless backhaul," *IEEE Transactions on Vehicular Technology*, vol. 69, no. 1, pp. 663–675, Jan. 2020.

[39] A. Alkhateeb and R. W. Heath, "Frequency selective hybrid precoding for limited feedback millimeter wave systems," *IEEE Transactions on Communications*, vol. 64, no. 5, pp. 1801–1818, May 2016.

[40] P. Schniter and A. Sayeed, "Channel estimation and precoder design for millimeter-wave communications: The sparse way," in *2014 48th Asilomar Conference on Signals, Systems and Computers*, Nov. 2014, pp. 273–277.

[41] J. A. Rice, *Mathematical Statistics and Data Analysis.*, 3rd ed. Belmont, CA: Duxbury Press., 2006.

[42] S. Verdu, "Spectral efficiency in the wideband regime," *IEEE Transactions on Information Theory*, vol. 48, no. 6, pp. 1319–1343, June 2002.

[43] J. Benesty, J. Chen, and Y. Huang, *Microphone Array Signal Processing: Conventional Beamforming Techniques*. Springer Berlin Heidelberg, 2008.

[44] *Study on channel model for frequencies from 0.5 to 100 GHz (Release 15)*, 3GPP Std. 38.901, 2018.

Kun Chen-Hu received his Ph.D. degree in Multimedia and Communications in 2019 from Universidad Carlos III de Madrid (Spain). Currently, he is a post-doctoral researcher in the same institution. He was also awarded by the same institution in 2019 recognizing his outstanding professional career after graduation. He visited Eurecom (France) and Vodafone Chair TU Dresden (Germany), both as guest researcher. He also participated in different research projects in collaboration with several top companies in the area of mobile communications. His research interests are related to signal processing techniques, such as waveforms design, non-coherent massive MIMO and channel estimation.

Yong Liu Yong Liu received the Ph.D in electronic engineering from the Department of Electric Engineering, Shanghai Jiao Tong University, Shanghai, China, in 2012. He is now with the wireless network RAN research department in Huawei Technologies Co.,Ltd., Shanghai, China. His current research interests lie in the area of 5G and 5G+ MIMO communication and AI assisted wireless networks.

Ana García Armada (S'96-A'98-M'00-SM'08) received the Ph.D. degree in electrical engineering from the Polytechnical University of Madrid in February 1998. She is currently a Professor at University Carlos III of Madrid, Spain. She is leading the Communications Research Group at this university. She has been visiting scholar at Stanford University, Bell Labs and University of Southampton. She has participated (and coordinated most of them) in more than 30 national and 10 international research projects as well as 20 contracts with the industry, all of them related to wireless communications. She is the co-author of eight book chapters on wireless communications and signal processing. She has published around 150 papers in international journals and conference proceedings and she holds four patents. She has contributed to international standards organizations, such as ITU and ETSI, and is member of the expert group of the European 5G PPP and member of the advisory committee 5JAC of the ESA as expert appointed by Spain on 5G. She has served on the editorial boards of Physical Communication (2008-2017), IET Communications (2014-2017). She has been serving on the editorial board of IEEE Communications Letters since 2016 (Editor until Feb 2019, Senior Editor from Mar 2019, Exemplary Editor Award 2017 and 2018) and IEEE Transactions on Communications since 2019. She has served on the TPC of more than 40 conferences and she has been member of the organizing committee of IEEE Globecom 2019, IEEE Vehicular Technology Conference (VTC) Fall 2018, Spring 2018 and 2019 and IEEE 5G Summit 2017, among others. She will be the General Chair of Globecom 2021. She was the Newsletter Editor of the IEEE ComSoc Signal Processing and Consumer Electronics Committee (2017-2018) and is now the Secretary of this committee (since 2019). She has been the Secretary of the IEEE ComSoc Women in Communications Engineering Standing Committee (2016-2017) and the Chair of this committee (2018-2019). She has received the Young Researchers Excellence Award, the Award to Outstanding achievement in research, teaching and management and the Award to Best Practices in Teaching, all from University Carlos III of Madrid, She was awarded the third place Bell Labs Prize 2014 for shaping the future of information and communications technology. She received the Outstanding service award from the IEEE ComSoc Signal Processing and Communications Electronics (SPCE) technical committee in 2019. Her main interests are multi-carrier and multi-antenna techniques and signal processing applied to wireless communications.